

A High Power-Density Mediator-Free Microfluidic Biophotovoltaic Device for Cyanobacterial Cells

Paolo Bombelli,^{1, a)} Thomas Müller,^{2, a)} Therese W. Herling,² Christopher J. Howe,^{1, b)} and Tuomas P. J. Knowles^{2, c)}

¹⁾Department of Biochemistry, University of Cambridge, Tennis Court Road, Cambridge CB2 1QW, United Kingdom

²⁾Department of Chemistry, University of Cambridge, Lensfield Road, Cambridge CB2 1EW, United Kingdom

Biophotovoltaics has emerged as a promising technology for generating renewable energy since it relies on living organisms as inexpensive, self-repairing and readily available catalysts to produce electricity from an abundant resource - sunlight. The efficiency of biophotovoltaic cells, however, has remained significantly lower than that achievable through synthetic materials. Here, we devise a platform to harness the large power densities afforded by miniaturised geometries. To this effect, we have developed a soft-lithography approach for the fabrication of microfluidic biophotovoltaic devices that do not require membranes or mediators. *Synechocystis sp.* PCC 6803 cells were injected and allowed to settle on the anode, permitting the physical proximity between cells and electrode required for mediator-free operation. We demonstrate power densities of above 100 mW/m² for a chlorophyll concentration of 100 μM under white light, a high value for biophotovoltaic devices without extrinsic supply of additional energy.

Fuelling the ever-growing need for energy¹ by fossil combustibles is expected to have dramatic, global consequences on climate and ecosystems. These environmental effects, in combination with the depletion of fossil fuel reserves, have led to a pressing need for developing technologies for harnessing renewable energy.^{2,3} In this scenario, bio-electrochemical systems - such as microbial fuel cells⁴⁻⁷ (MFCs) and biological photovoltaic cells⁸⁻¹² (BPVs) - may help to alleviate the present concerns by utilising living organisms as inexpensive, readily available catalysts to generate electricity. A particularly advantageous feature of BPVs is that they consist of living photosynthetic material that allows for continuous repair of photo-damage to key proteins.

Whereas MFCs use heterotrophic bacteria to convert the chemical energy stored in organic matter, BPVs use photosynthetic organisms capable of harnessing solar energy. In MFCs operating with *Geobacter sulfurreducens*, the oxidation of acetate can proceed with a Coulombic efficiency of ~ 100%.¹³ Nevertheless, the availability of acetate and other organic substrates is not endless which imposes a limiting factor to this approach. By contrast, in BPV-type systems, the conversion efficiencies of light into charges remain low (~ 0.1%),¹⁴ but the primary fuel (i.e., solar light) is virtually unlimited. Consequently, a significant research effort is required towards understanding which processes limit the performance of biophotovoltaic cells, both in terms of biophysics and engineering.

In this context, miniaturisation of BPVs provides highly attractive possibilities for high-throughput studies of small cell cultures, down to individual cells, in order to learn about differences in genetically identical organ-

isms as well as to direct the evolution of efficient cell lines in bulk¹⁵⁻¹⁷ and in microfluidics.¹⁸ Furthermore, the distances which the charge carriers have to migrate within the devices can be shortened dramatically, reducing resistive losses in the electrolyte.⁴ The readily achievable conditions for laminar flow and sessile state of the anodophilic photosynthetic cells also permit operation without the use of a proton-exchange membrane.¹⁹⁻²²

To date, efforts have focussed on miniaturised microbial fuel cells.^{7,22-30} In order to exploit the high power densities available through the decrease of the length scales of the charge transport and the decrease of the electrolyte volume, we have developed a simple fabrication method for microfluidic biophotovoltaic (μBPV) devices²³ that do not require an electron mediator or a proton-exchange membrane. Besides increasing efficiency and simplicity of the device, relinquishing mediator and membrane also reduces the cost of potential large-scale applications.^{14,31-33}

We use soft lithography³⁴ to form microscopic channels which we equip using microsolidics³⁵ with a self-aligned electrode from a low-melting point alloy^{1,3,37} (InSnBi) and a platinum electrode sealed inside microfluidic tubing. A scheme of such a device is shown in Fig. 1(a-c), and the specific design including the external measurement circuit is presented in Fig. 1(d). True-colour microscopy photographs of a device filled with Coomassie blue, with freshly injected *Synechocystis* cell, as well as with cells that have settled on the anode during 24 hours are shown in Fig. 1(e), (f), and (g), respectively. The possibility of omitting the mediator arises from the physical proximity of the settled cells and the anode which forms the bottom of the device, as well as the choice of electrode materials. The latter ensures that H⁺ is preferably reduced at the cathode since platinum catalyses this reaction.

The inherently small size (below 400 nL) of our mi-

^{a)}These authors contributed equally to this work.

^{b)}Electronic mail: ch26@cam.ac.uk

^{c)}Electronic mail: tpjk2@cam.ac.uk

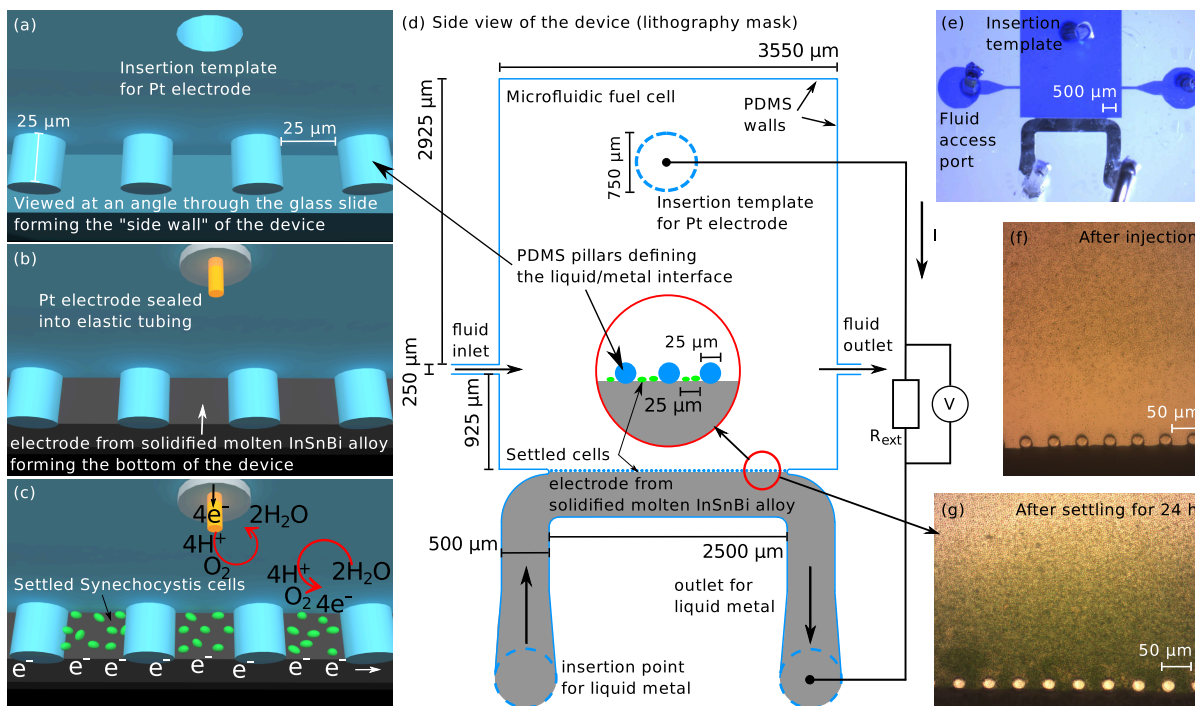


FIG. 1. (a) Schematic of the device before insertion of the electrodes, seen at an angle through the glass slide. The lithographically defined PDMS pillars retain molten metal due to its surface tension, and the hole provides an opening for insertion of the Pt electrode. (b) Model of the full device including platinum cathode and InBiSn anode. (c) Schematic representation of the microfluidic biophotovoltaic device in action. *Synechocystis* cells settled by gravity on the InBiSn electrode deliver electrons to the latter by oxidising water. On the platinum cathode oxygen and hydrogen ions are supplied with electrons and combine to water, which closes the circuit. (d) Top view of the device design. (e) True-colour image of a device filled with a solution containing Coomassie blue to visualise the 25 μm high channels. (f) True-colour image of a device immediately after injection of *Synechocystis* cells at a chlorophyll concentration of around 100 μM . (g) True-colour image of a device filled with *Synechocystis* cells that were allowed to settle on the anode during 24 h.

crofluidic approach permits studies of minute amounts of biological material. Moreover, our μBPV works without any additional energy supply, such as inert gas purging to keep the anodic chamber anoxic and/or oxygen gas purging in the cathodic chamber to facilitate the reformation of water,^{8,39,40} or a bias potential applied to polarise the electrodes and improve the electron flux between anode and cathode.³³

The use of soft lithography allows for fast in-house prototyping and for the utilisation of the range of techniques developed for integrated circuits. Despite the small volumes contained in microfluidic devices, such approaches can be scaled up by parallelisation,^{30,41} and the surface-to-volume ratio can be designed to outperform macroscopic approaches significantly.²⁹

RESULTS

The microfluidic BPV device described here operates as a microbial fuel cell with submicroliter volume, generating electrical power by harnessing the photosynthetic and metabolic activity of biological material. Its anodic

half-cell consists of sessile *Synechocystis* cells - performing water photolysis ($2\text{H}_2\text{O} \rightarrow 4\text{H}^+ + 4\text{e}^- + \text{O}_2$) and subsequent “dark” metabolism - as well as an anode made from an InSnBi alloy and a light source.

Current and power analyses

A μBPV was loaded with wild type *Synechocystis* *sp.* PCC 6803 cells (subsequently referred to as *Synechocystis*) suspended in BG11 medium - supplemented with NaCl - at a final chlorophyll concentration of 100 nmol Chl mL^{-1} . The exoelectrogenic activity of three biological replicates of sessile cells was characterised under controlled temperature conditions sequentially in the same device.

The μBPV was rested for 24 hours, permitting the formation of cellular films on the anodic surface and stabilising the open circuit potential. Polarisation and power curves were then recorded by connecting different resistance loads to the external circuit in the dark or under illumination with white LED light (see Methods), and are shown in Fig. 2.

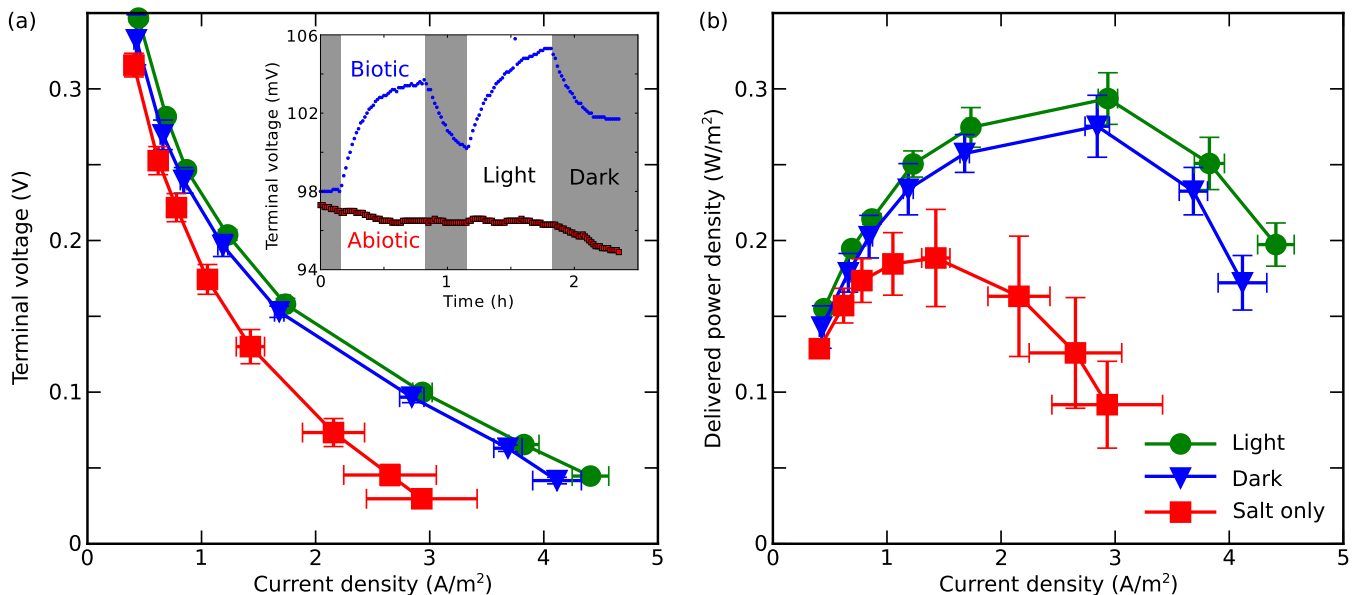


FIG. 2. (a) Comparison of the voltage output from the same microfluidic device loaded with salt medium only (BG11) or *Synechocystis* cells in medium in the dark and with light. The x -axis has been converted to a current density through division of the measured current by the surface of the InSnBi anode, and the error bars show the standard deviations for three consecutive, independent repeats on the same device. Inset: Response of the biophotovoltaic device as well as of an abiotic control under sequential illumination. (b) Power density generated by the microfluidic devices filled with salt or cells in dark/illuminated environment.

In the dark, significant power output was observed relative to the control sample containing no cells. This observation is consistent with the breakdown of stored carbon intermediates accumulated during the light period.¹¹ The peak power output of $275 \pm 20 \text{ mW m}^{-2}$ was established at a current density of $2840 \pm 110 \text{ mA m}^{-2}$. Under illumination the microfluidic BPV loaded with *Synechocystis* showed an increase in both current and power output. The peak power density was $P/A = 294 \pm 17 \text{ mW m}^{-2}$ established at a current of $2940 \pm 85 \text{ mA m}^{-2}$. Crucially, both the dark and the light electrical outputs were significantly higher than the abiotic peak power output in this device of $189 \pm 32 \text{ mW m}^{-2}$ established at a current of $1430 \pm 120 \text{ mA m}^{-2}$, demonstrating that the power output from our devices originates from the biological activity of the cyanobacteria.

From the linear slope at the high current side of the polarization curve as well as the from the external resistance for which maximal power transfer occurs we can estimate the internal resistance of the device to be around $2.2 \text{ M}\Omega$ for the biotically loaded device and $1.4 \text{ M}\Omega$ for the abiotic control (for further details see Supplementary Material).

The electrical output recorded from the abiotic control - possibly due to medium salinity^{5,42} and anodic oxidation - is taken into account when the power densities of biotic experiments are quoted. Specifically, subtracting the abiotic background yields a biotic output power density of 105 mW m^{-2} . This number is halved when comparing to the full cross-sectional area of the device

(including the inaccessible parts of the anode), and the power available per footprint area is ca. $50 \mu\text{W m}^{-2}$.

Light response

To demonstrate the photo-activity of the *Synechocystis* cells, the variation of the anode-cathode voltage as a response to repeated light stimulation was recorded over time (see inset of Fig. 2(a)). The external resistor was fixed at $100 \text{ M}\Omega$, and the voltage was sampled once per minute. Illumination by white LED light at $200 \mu\text{mol m}^{-2}\text{s}^{-1}$ resulted in a reproducible voltage increase at a rate of $21.7 \pm 4.7 \text{ mV h}^{-1}$ with $\Delta V_{\text{light-dark}} = 5.2 \pm 0.6 \text{ mV}$. The time until the electrical outputs were stabilised was around one hour. We find that the baseline voltage levels change after illumination - most certainly due to a buildup and breakdown of intracellular metabolites.

From the measured spectrum of the light source (see Supplementary Information) we can determine the average wave number which corresponds to a wavelength of 570 nm . Thus the photon flux can be converted to an incident light intensity of 42 W m^{-2} . Using these values we can extract a rough estimate for the efficiency of our BPV (energy output versus energy input) of around 0.25% which compares favourably to previously achieved values.^{14,23,43} Note that light scattering on the glass surface and losses from the non perpendicular illumination angle would increase this number and hence it can be

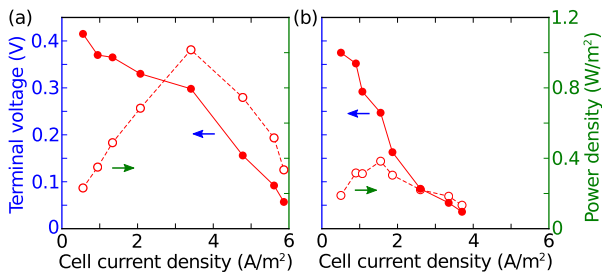


FIG. 3. (a) and (b) Output voltage (filled circles, solid line, blue axis) and available power density (hollow circles, dashed line, green axis) as a function of current from two further abiotically loaded devices (BG11 cell medium supplemented with 0.25 M NaCl).

understood as a lower bound.

With such an illumination cycle, the light-driven electrical response of a device can be directly compared to dark conditions, proving the functionality of our μ BPV. In addition, the abiotic control shows no variations in anode-cathode potential under similar illumination.

The difference between the power outputs under dark and illuminated conditions is consistent with previous studies of *Synechocystis sp.* PCC 6803.¹⁴ Nevertheless, a direct comparison of the power output reported by McCormick *et al.* of around 0.12 mW m^{-2} with the peak value in excess of 100 mW m^{-2} demonstrated here emphasises the great potential of microfluidic approaches compared to macroscopic devices.

Variability of the abiotic characterisation

In order to characterise the variability of the electrical behaviour of our μ BPV, two further, lithographically identical devices were studied with abiotic loading (i.e., without photosynthetic cells). These devices were injected with BG11 media (with 0.25 M NaCl), and the current and power outputs were characterised under controlled temperature conditions.

Following 24 hours of stabilisation of the μ BPV at open circuit potential, polarisation and power curves (see Fig. 3) were generated by applying different resistance loads to the external circuit in the dark. In different devices, the abiotic peak power density outputs vary from around 0.2 to 1 W/m^2 and were established at current densities of 1.5 and 3.5 A/m^2 , respectively. The large variation in device output between different devices stems from the variable position and shape of the cathode which is not lithographically defined in our current designs. Device improvements at this level may well provide a straightforward route to further improvement of the output power. Crucially, no major changes in current and power outputs were observed upon exposure to white light (see inset of Fig. 2(a)).

Comparison with recent literature

The exceptionally high power density in excess of 100 mW m^{-2} after subtraction of the abiotic background has been facilitated by the physical proximity of the cells to the anode allowing for operation without a proton-exchange membrane, which in turn leads to a low internal resistance in the device, as well as by the microscopic size of the anodic chamber allowing for a large ratio of active surface to volume. In macroscopic bio-electrochemical systems by contrast, parameters such as mass transport, reaction kinetics and ohmic resistance are expected to have detrimental effect on the electrical output.^{4,29}

For a specific comparison, Tab. I gives an overview of the power densities as well as technical specifications of intrinsic BPVs (i.e., requiring no external energy) characterised in the recent literature, including an instance with an additional enzymatic cathode.⁵⁰ While there are many aspects influencing the performance of a BPV, such as surface-to-volume ratio, photosynthetic organism, and electrode material, one can observe a trend that generally the mediator-free approaches surpass their counterparts that rely on electron mediators diffusing over large distances. It should be mentioned that many of the studies listed in Tab. I were not intended to improve on output power. We also note that higher power densities have been observed⁸ when extrinsic energy was supplied.

DISCUSSION

In summary, we have described a microfluidic design for a mediator-less, membrane-free bio-photovoltaic device. Electrical characterisation of devices loaded with *Synechocystis sp.* PCC 6803 revealed peak power densities in excess of 100 mW/m^2 . In spite of the low power available per footprint area (currently of the order of $50 \mu\text{W/m}^2$) the promising performance and the simple fabrication process demonstrate the potential of our approach for generating biological solar cells with microfluidics.

Our approach is applicable to any photosynthetic organism forming biofilms. Furthermore, using the strategy presented in this work, further improvement of the power output should be readily achievable through reduction of the distance between anode and cathode and increase of the channel height. This flexibility in device geometry and the possibility of *in-situ* electroplating of the anode underline the versatility of soft-lithography as a means for generating biophotovoltaic cells.

Options for enhanced miniaturisation open pathways for the study of small cell cultures containing as little as tens of cells for rapid screening of electrochemically active microbes in the context of directed evolution.

Study	P_{out} mW/m ²	AAA mm ²	ACV μ L	Anode/ Cathode	Mediator	Photosynthetic organism
Chiao 2006 ²³	0.0004	50	4.3	Au/ N-Au - csc	Methylene blue	<i>Anabaena sp.</i>
Bombelli 2011 ¹¹	1.2	80	150	ITO/N-CPt	K ₃ [Fe(CN) ₆]	<i>Synechocystis sp.</i> PCC 6803
McCormick 2011 ¹⁴	10	1'300	12'600	ITO/ Pt-coated glass	free	<i>Synechococcus sp.</i> WH 5701
Thorne 2011 ⁴⁴	24	230	2'300	FTO/Carbon cloth	K ₃ [Fe(CN) ₆]	<i>Chlorella vulgaris</i>
Bombelli 2012 ⁴⁵	0.02	2'000	20'000	ITO/Pt-C	free	<i>Oscillatoria limnetica</i>
Madiraju 2012 ⁴⁶	0.3	1'500	60'000	Carbon fibre	free	<i>Synechocystis sp.</i> PCC 6803
Bradley 2013 ⁴⁷	0.2	1'300	31'500	ITO/N-CPt	K ₃ [Fe(CN) ₆]	<i>Synechocystis TM</i>
Lan 2013 ⁴³	13	4'600	5 × 10 ⁵	Pre-treated graphite/csc	K ₃ [Fe(CN) ₆]	<i>Chlamydomonas reinhardtii</i>
Lin 2013 ⁴⁸	10	2'100	10 ⁶	Au mesh/Graphite cloth	free	<i>Spirulina platensis</i>
Luimstra 2013 ⁴⁹	6	1'400	70'000	PPCP/ Carbon cloth with Pt	free	<i>Pauschulzia pseudovolvox</i>
Sekar 2014 ⁵⁰	35	2.5	n/a	CNTCP/ Laccase on CNTCP	free	Nostoc sp.
Sekar 2014 ⁵⁰	100	2.5	n/a	CNTCP/ Laccase on CNTCP	BQ	Nostoc sp.
This study	105	0.03	0.4	InSnBi alloy/Pt	free	<i>Synechocystis sp.</i> PCC 6803

TABLE I. List of biophotovoltaic devices from the recent literature - including previous microfluidic approaches - that do not require additional energy input. The abbreviations used are anodic active area (AAA), anodic chamber volume (ACV), Nafion film over the cathodic chamber and Au cathode (N-Au), chemical sacrificial cathode (csc), carbon-platinum cathode impregnated on one side with Nafion (N-CPt), carbon paper coated with a thin layer of platinum (Pt-C), indium tin oxide (ITO), fluorine doped tin oxide (FTO), carbon paint with polypyrrole (PPCP), carbon nanotubes on carbon paper (CNTCP), and benzoquinone (BQ). *Synechocystis TM* refers to mutant strains of the cyanobacterium *Synechocystis sp.* PCC 6803 where the three respiratory terminal oxidase complexes had been inactivated.

METHODS

Device fabrication

Devices were fabricated to a height of 25 μ m using standard soft lithography³⁴ for polydimethylsiloxane (PDMS) on glass. The designs include an array of 25 μ m wide PDMS pillars spaced by 25 μ m in order to allow for insertion of molten solder^{1,37} (Indalloy 19, Indium Corporation, Clinton NY, USA) on a hotplate set to 79 °C. Solidification of this InBiSn alloy upon removal from the heat yields self-aligned wall electrodes using a single lithography step.³ This process is illustrated in Fig. 1(a) and (b). The cathode is constructed by inserting a strip of platinum wire of 100 μ m diameter through polyethylene tubing (Smiths Medical; 800/100/120; the same as used for contacting microfluidic devices in general) and sealing off both ends of the tubing with epoxy glue. Inserting this tube through a previously punched hole in the device generates a sealed electrical connection and is indicated by the orange wire (Pt) inside a white cylinder (tubing) in the scheme in Fig. 1(b). Note that this method for electrode fabrication also allows for straightforward exchange of the cathode material, which would be beneficial for *in-situ* electroplating the InBiSn alloy.

During settling and operation, the BPVs are oriented such that the bottom of the device is formed by the anode, and

the glass slide as well as the pdms forming the side and top walls.

The total volume above the anode is below 400 nL, significantly reducing the consumption of biological material and chemicals of each experiment compared to macroscopic approaches.

Electrode Area

The accessible surfaces of these electrodes are ca. $A \sim 2.5 \text{ mm}/2 \times 25 \mu\text{m} \approx 0.03 \text{ mm}^2$ for the anode (only approximately one half of the total metal area is accessible due to the PDMS pillars) and of the order of 0.6 mm^2 for the cathode, assuming the available length of the Pt wire to be 2 mm. Note that the majority of the cathode lies inside the cavity of the insertion template. If one were to consider the entire horizontal cross-section of the device, the according area would double to 0.06 mm^2 , and the footprint of the device is at present around 60 mm^2 including the access ports for fluid injection. This latter number can be reduced straightforwardly by more than one order of magnitude by redesigning the inlet ports.

Cell culture and growth

A wild-type strain of *Synechocystis sp.* PCC 6803 was cultivated from a laboratory stock.¹¹ Cultures were grown and then analysed in BG11 medium⁵¹ supplemented with 0.25 M NaCl. All cultures were supplemented with 5 mM NaHCO₃ and maintained at 22 ± 2 °C under continuous low light (ca. 50 μmol m⁻²s⁻¹) in sterile conditions. Strains were periodically streaked onto plates containing agar (0.5–1.0%) and BG11 including NaCl, which were then used to inoculate fresh liquid cultures. Culture growth and density were monitored by spectrophotometric determination of chlorophyll content. Chlorophyll was extracted in 99.8% (v/v) methanol (Sigma-Aldrich, Gillingham, UK) as described previously.⁵²

Cell injection and settling

First, the devices were filled with culture medium (BG11 with 0.25 M NaCl) and any air bubbles were removed by means of syringes attached via elastic polyethylene tubing (Smiths Medical; 800/100/120). *Synechocystis* cells suspended in BG11 (supplemented with NaCl) were then injected at a concentration of 100 μM chlorophyll. Maintaining the devices for 24 h at an orientation in which the metal alloy anode forms the bottom allows the cells to sediment on the electrode by gravity. This process creates a closely-spaced interface allowing the electrons to be transmitted to the anode (see Fig. 1(c) and (g)) and thus favouring mediator-free operation. Throughout all experiments, the syringes are kept attached in order to prevent drying out of the BPV.

The complete device design used for the photolithography mask is presented in Fig. 1(d), and a microscopy photograph of a device coloured with Coomassie blue is shown in Fig. 1(e). Furthermore, a picture of an array of devices is provided in the supplementary material.

Microfluidic BPV measurement and illumination

In principle, the optimal way of extracting the voltage output of our biophotovoltaic device would be to determine the half-cell potentials individually by integrating reference electrodes into the devices. Since this is challenging in microfluidic devices,⁵³ we have instead measured the terminal voltage of our BPV which does not offer insight into the potentials of the complex half-cell reactions but provides an accurate measurement for the power delivered to an external load.

Polarisation curves were acquired by recording the terminal voltage V under pseudo steady-state conditions⁵ with variable external loads (R_{ext}) and plotting the cell voltage as a function of current density (current per unit anodic area). Typically, a time span of around 20 min was sufficient for a stable output (see Supplementary Fig. 2). The resistance values ranged from 24.8 MΩ to 324 kΩ (24.8, 13, 9.1, 5.3, 2.9, 1.1, 0.547, and 0.324 MΩ), where the internal resistance of the digital voltmeter of 100 MΩ has been taken into account. Voltages were recorded using an UT-70 data logger (Uni-Trend Limited, Hong Kong, China). The current delivered to the load was calculated from Ohm's law

$$V = R_{\text{ext}}I, \quad (1)$$

and the power P is given by

$$P = V^2/R_{\text{ext}}. \quad (2)$$

Based on the polarisation curves, power curves were obtained for each system by plotting the power per unit area or power density P/A as a function of current density. These power density curves were further used to determine the average maximum power output for the microfluidic BPV system and the negative control. For all measurements, alligator clamps and copper wire served as connections to anode and cathode, and the temperature was kept at 22 ± 2 °C.

To characterise the light response, artificial light was provided by a warm white LED bulb (Golden Gadgets, LA2124-L-A3W-MR16), maintained at a constant output of 200 μmol m⁻²s⁻¹ at the location of the BPVs. A measured spectrum of the light source is shown in the supplementary material. Light levels were measured in μmol m⁻²s⁻¹ with a SKP 200 Light Meter (Skye Instruments Ltd, Llandrindod Wells, UK).

The photo-active cells were illuminated through the glass slide forming the bottom of the device, resulting in an almost parallel angle of incidence on the cell layer. This geometry does lead to a decreased light intensity on the cells, which may be compensated for by using a more powerful light source in studies of photosynthetic materials or by altering the geometric arrangement of the devices when harnessing actual sunlight.

REFERENCES

- ¹U.S. Energy Information Administration, *International Energy Outlook 2013*.
- ²N. S. Lewis and D. G. Nocera, *Proc Natl Acad Sci USA* **103**, 15729 (2006).
- ³M. New, D. Liverman, H. Schroeder, and K. Anderson, *Phil Trans Royal Soc A* **369**, 6 (2011).
- ⁴K. Rabaey and W. Verstraete, *Trend Biotech* **23**, 291 (2005).
- ⁵B. E. Logan, B. Hamelers, R. Rozendal, U. Schröder, J. Keller, S. Freguia, P. Aelterman, W. Verstraete, and K. Rabaey, *Envir Sci Technol* **40**, 5181 (2006).
- ⁶Y. Yang, G. Sun, and M. Xu, *J Chem Tech Biotech* **86**, 625 (2011).
- ⁷X. Jiang, J. Hu, E. R. Petersen, L. A. Fitzgerald, C. S. Jackan, A. M. Lieber, B. R. Ringeisen, C. M. Lieber, and J. C. Biffinger, *Nat Commun* **4**, 2751 (2013).
- ⁸S. Tsujimura, A. Wadano, K. Kano, and T. Ikeda, *Enzyme Microbial Tech* **29**, 225 (2001).
- ⁹M. Rosenbaum, U. Schröder, and F. Scholz, *Appl Microbiol Biotech* **68**, 753 (2005).
- ¹⁰J. M. Pisciotta, Y. Zou, and I. V. Baskakov, *PLoS One* **5**, e10821 (2010).
- ¹¹P. Bombelli, R. W. Bradley, A. M. Scott, A. J. Philips, A. J. McCormick, S. M. Cruz, A. Anderson, K. Yunus, D. S. Bendall, P. J. Cameron, J. M. Davies, A. G. Smith, C. J. Howe, and A. C. Fisher, *Energy Environ Sci* **4**, 4690 (2011).
- ¹²N. Samsonoff, M. D. Ooms, and D. Sinton, *Appl Phys Lett* **104**, 043704 (2014).
- ¹³K. P. Nevin, H. Richter, S. F. Covalla, J. P. Johnson, T. L. Woodard, A. L. Orloff, H. Jia, M. Zhang, and D. R. Lovley, *Environ Microbiol* **10**, 2505 (2008).
- ¹⁴A. J. McCormick, P. Bombelli, A. M. Scott, A. J. Philips, A. G. Smith, A. C. Fisher, and C. J. Howe, *Energy Environ Sci* **4**, 4699 (2011).
- ¹⁵P. J. Carter, *Nat Rev Immun* **6**, 343 (2006).
- ¹⁶S. Bershtein and D. S. Tawfik, *Curr Opin Chem Biol* **12**, 151 (2008).

- 17 J. D. Keasling, *ACS Chem Biol* **3**, 64 (2008).
- 18 J. Agresti, E. Antipov, A. Abate, K. Ahn, A. Rowat, J. Baret, M. Marquez, A. Klibanov, A. Griffiths, and D. Weitz, *Proc Natl Acad Sci USA* **107**, 4004 (2010).
- 19 E. R. Choban, L. J. Markoski, A. Wieckowski, and P. J. A. Kenis, *J of Power Sources* **128**, 54 (2004).
- 20 E. Kjeang, N. Djilali, and D. Sinton, *J Power Sources* **186**, 353 (2009).
- 21 H.-Y. Wang and J.-Y. Su, *Bioresource Tech* **145**, 271 (2013).
- 22 D. Ye, Y. Yang, J. Li, X. Zhu, Q. Liao, B. Deng, and R. Chen, *Intl J Hydr Energy* **38**, 15710 (2013).
- 23 M. Chiao, K. B. Lam, and L. Lin, *J Micromech Microeng* **16**, 2547 (2006).
- 24 S. R. Crittenden, C. J. Sund, and J. J. Sumner, *Langmuir* **22**, 9473 (2006).
- 25 C.-P. Siu and M. Chiao, *J Microelectromech Sys* **17**, 1329 (2008).
- 26 H. Hou, L. Li, Y. Cho, P. de Figueiredo, and A. Han, *PLoS One* **4**, e6570 (2009).
- 27 F. Qian, M. Baum, Q. Gu, and D. E. Morse, *Lab Chip* **9**, 3076 (2009).
- 28 F. Qian, Z. He, M. P. Thelen, and Y. Li, *Bioresource Technology* **102**, 5836 (2011).
- 29 H.-Y. Wang, A. Bernarda, C.-Y. Huang, D.-J. Lee, and J.-S. Chang, *Bioresource Tech* **102**, 235 (2011).
- 30 H. Hou, L. Li, C. U. Ceylan, A. Haynes, J. Cope, H. H. Wilkinson, C. Erbay, P. d. Figueiredo, and A. Han, *Lab Chip* **12**, 4151 (2012).
- 31 D. R. Bond and D. R. Lovley, *Appl Environ Microbiol* **69**, 1548 (2003).
- 32 G. Reguera, K. P. Nevin, J. S. Nicoll, S. F. Covalla, T. L. Woodard, and D. R. Lovley, *Appl Environ Microbiol* **72**, 7345 (2006).
- 33 S. Malik, E. Drott, P. Grisdela, J. Lee, C. Lee, D. A. Lowy, S. Gray, and L. M. Tender, *Energy Environ Sci* **2**, 292 (2009).
- 34 J. McDonald and G.M. Whitesides, *Acc Chem Res* **35**, 491 (2002).
- 35 A. C. Siegel, D. A. Bruzewicz, D. B. Weibel, and G. M. Whitesides, *Adv Mater* **19**, 727 (2007).
- 1 J.-H. So and M. D. Dickey, *Lab Chip* **11**, 905 (2011).
- 37 S. Li, M. Li, Y. Hui, W. Cao, W. Li, and W. Wen, *Microfluid Nanofluid* **14**, 499 (2013).
- 3 T. W. Herling, T. Müller, L. Rajah, J. N. Skepper, M. Vendruscolo, and T. P. J. Knowles, *Appl Phys Lett* **102**, 184102 (2013).
- 39 T. Yagishita, S. Sawayama, K.-I. Tsukahara, and T. Ogi, *Bioelectrochem Bioenerg* **43**, 177 (1997).
- 40 M. Torimura, A. Miki, A. Wadano, K. Kano, and T. Ikeda, *J Electroanal Chem* **496**, 21 (2001).
- 41 M. B. Romanowski, A. R. Abate, A. Rotem, C. Holtze, and D. A. Weitz, *Lab Chip* **12**, 802 (2012).
- 42 B. E. Logan, *Nat Rev Microbiol* **7**, 375 (2009).
- 43 J. C.-W. Lan, K. Raman, C.-M. Huang, and C.-M. Chang, *Biochem Eng J* **78**, 39 (2013).
- 44 R. Thorne, H. Hu, K. Schneider, P. Bombelli, A. Fisher, L. M. Peter, A. Dent, and P. J. Cameron, *J Mater Chem* **21**, 18055 (2011).
- 45 P. Bombelli, M. Zarrouati, R. J. Thorne, K. Schneider, S. J. L. Rowden, A. Ali, K. Yunus, P. J. Cameron, A. C. Fisher, D. Ian Wilson, C. J. Howe, and A. J. McCormick, *Phys Chem Chem Phys* **14**, 12221 (2012).
- 46 K. S. Madiraju, D. Lyew, R. Kok, and V. Raghavan, *Bioresource Tech* **110**, 214 (2012).
- 47 R. W. Bradley, P. Bombelli, D. J. Lea-Smith, and C. J. Howe, *Phys Chem Chem Phys* **15**, 13611 (2013).
- 48 C.-C. Lin, C.-H. Wei, C.-I. Chen, C.-J. Shieh, and Y.-C. Liu, *Bioresource Tech* **135**, 640 (2013).
- 49 V. M. Luimstra, S.-J. Kennedy, J. Güttler, S. A. Wood, D. E. Williams, and M. A. Packer, *J Appl Phycol* **26**, 15 (2013).
- 50 N. Sekar, Y. Umasankar, and R. P. Ramasamy, *Phys Chem Chem Phys* **16**, 7862 (2014).
- 51 R. Rippka, J. Deruelles, J. Waterbury, M. Herdman, and R. Stanier, *J Gen Microbiol* **111**, 1 (1979).
- 52 R. Porra, W. Thompson, and P. Kriedemann, *Biochim Biophys Acta* **975**, 384 (1989).
- 53 M. W. Shinwari, D. Zhitomirsky, I. A. Deen, P. R. Selvaganapathy, M. J. Deen, and D. Landheer, *Sensors* **10**, 1679 (2010).

ACKNOWLEDGEMENTS

We gratefully acknowledge financial support from the Biotechnology and Biological Sciences Research Council (BB-SRC), the Engineering and Physical Sciences Research Council (EPSRC), the European Research Council (ERC), the EnAlgae consortium (<http://www.enalgae.eu/>), as well as the Swiss National Science Foundation (SNF).

SUPPLEMENTARY INFORMATION

A. Device Handling

Figure 4 illustrates the operation of the device. After the fabrication of the device and the electrodes, the cell medium is injected using plastic syringes, and all air is removed by applying pressure on the fluid inlet and outlet. Thereafter, the elastic tubing is cut on one side and the cells are injected through another syringe. The syringes are then left attached to prevent drying of the device. Copper wires are soldered to the electrodes to provide electric connections. Finally, the device is positioned such that the anode forms the bottom and the cells sediment on it under the influence of gravity.

A magnified version of a device filled with a Coomassie blue solution is shown in Fig. 5(a), and a true-colour microscopy image of *Synechocystis sp.* PC 6803 cells settled on the alloy anode is presented in Fig. 4(b).

B. Device stability

In order to assess the stability of our devices, a sample was loaded with cell medium and its power output was measured during more than 25 hours (see Fig. 6). After a sharp decrease in the first minutes, the device was stable for a period in excess of 24 hours.

C. Anode Material

The low-melting point solder Indalloy 19 (Indium Corporation, Clinton NY, USA) - composed of 51% indium, 32.5% bismuth, and 16.5% tin - has been chosen due to its simplicity for generating self-aligned wall electrodes in microfluidic devices.¹⁻³ The melting point at 60 °C enables straightforward insertion into the device on a hot plate at 79 °C, with the liquid metal patterned by polydimethylsiloxane pillars due

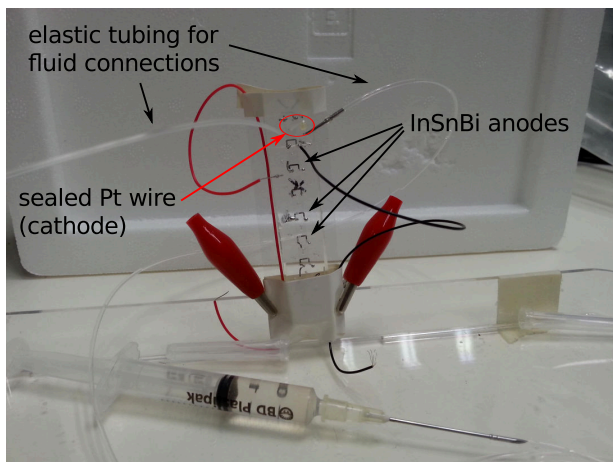


FIG. 4. Photograph of an array of devices. Anodes were fabricated for all cells, the sealed cathode and the fluid connectors are inserted into the topmost device.

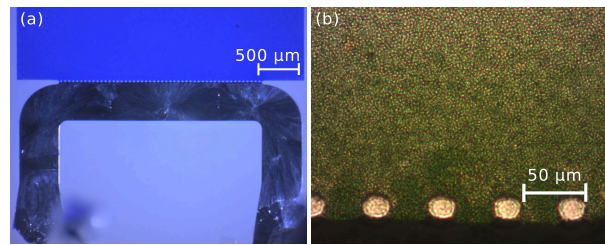


FIG. 5. (a) True-colour microscopy image of the indium alloy electrode and the fluid chamber filled with a Coomassie blue solution. (b) True-colour microscopy image of *Synechocystis sp.* PC 6803 cells settled on the alloy anode during 24 h.

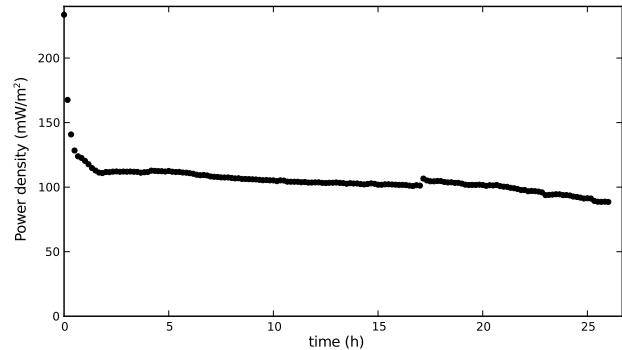
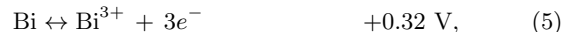


FIG. 6. Power output of an abiotically loaded device over an extended period of time, measured every 6 minutes.

to its surface tension. Upon removing the devices from the hot plate the alloy solidifies forming a solid electrode.

The standard potentials of each of the constituent metals are⁴



These potentials are below the value for the oxidation of hydrogen to water at the cathode (+1.23 V), and therefore it is quite possible that oxides such as, for instance, In_2O_3 , Bi_2O_3 , $\text{Bi}_2\text{Sn}_2\text{O}_7$, or SnO_2 are forming on the anode. We have subtracted this oxidative current from our power estimates and did not see any significant deterioration in performance in a control over a time span of 25 hours (Fig. 6).

D. Estimates of the internal resistance

Measuring the voltage drop over an external resistor attached to a source yields the terminal voltage which is smaller than the actual cell voltage due to the internal resistance of the source

$$V_{\text{terminal}} \equiv V = V_{\text{cell}} - R_{\text{int}}I = V_{\text{cell}} - \frac{R_{\text{int}}}{R_{\text{ext}}}V. \quad (7)$$

Therefore,

$$V = \frac{V_{\text{cell}}}{1 + R_{\text{int}}/R_{\text{ext}}}. \quad (8)$$

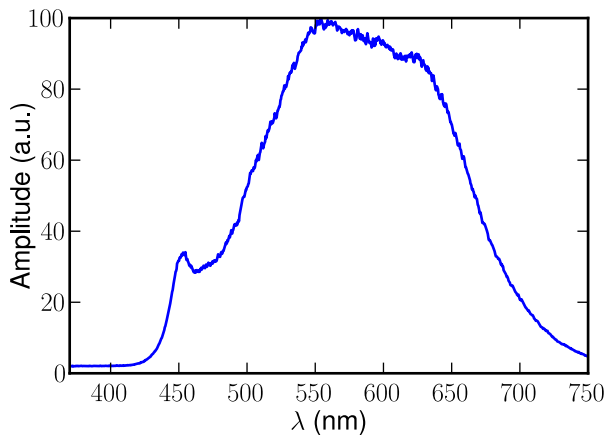


FIG. 7. Measured spectrum of the light source used in our experiments.

Since the IV -characteristics are not linear, the internal resistance of the cell, or - more likely - its output voltage, depends on the current drawn. Nevertheless, from the linear part of the polarisation curve at high currents (Fig. 2(a) in the main text) we can estimate the internal resistance to amount to

$$\frac{\Delta V}{\Delta I} \approx \frac{158 - 45 \text{ mV}}{(4.4 - 1.7 \text{ A/m}^2) * 0.03 \text{ mm}^2} = 1.4 \text{ M}\Omega \quad (9)$$

for the biotically loaded device and

$$\frac{\Delta V}{\Delta I} \approx \frac{130 - 30 \text{ mV}}{(2.9 - 1.4 \text{ A/m}^2) * 0.03 \text{ mm}^2} = 2.2 \text{ M}\Omega \quad (10)$$

for the abiotic control. Note that the internal resistance decreased by 1/3 with the addition of the cyanobacteria. Fur-

thermore, since maximal power transfer to the external load is observed when the load resistance is matched to the internal resistance of the cell, we can double-check the above values by comparison to Fig. 2(b). There, the maximum power is observed for external resistances of 1.1 M Ω and 2.9 M Ω for biotic and abiotic filling, respectively. These values are in close agreement with the estimates from the polarisation curves.

E. Light source

In Fig. 7 we present the measured spectrum of the lamp we have used to illuminate our biophotovoltaic cells. From these data, we can also extract the weighted average wave number to be 10^7 m^{-1} which corresponds to a wavelength of around 570 nm. Therefore, the average energy per photon is $3.5 \times 10^{-19} \text{ J}$, and the measured photon flux of $200 \mu\text{mol/m}^2/\text{s}$ yields an illumination intensity at the location of the devices of 42 W/m^2 .

Supplementary References

- ¹J.-H. So and M. D. Dickey, *Lab Chip*, 2011, **11**, 905–911.
- ²J. J. Li and C. M. Yip, *Biochimica et Biophysica Acta (BBA) - Biomembranes*, 2013, **1828**, 2272–2282.
- ³T. W. Herling, T. Müller, L. Rajah, J. N. Skepper, M. Vendruscolo and T. P. J. Knowles, *Appl Phys Lett*, 2013, **102**, 184102.
- ⁴*Standard Potentials in Aqueous Solution*, ed. A. J. Bard, R. Parsons and J. Jordan, CRC Press, 1985.